

Research article

Smart polyurethane composites: Magnetic-field-sensitive crosslinked shape-memory polyurethane composites

Berna Öztürk¹, Tugce Inan¹, Hüsnü Atakül¹, Fatma Seniha Guner^{1,2*}

¹Istanbul Technical University, Department of Chemical Engineering, Maslak 34469 Istanbul, Turkey

²Sabancı University Nanotechnology Research and Application Center (SUNUM), Tuzla 34956 Istanbul, Turkey

Received 12 September 2022; accepted in revised form 4 February 2023

Abstract. Smart polymers synthesized from renewable sources are precious because of the environmental pressures of producing polymers from fossil fuels. This study develops a new formulation of polyurethane (PU) from partly renewable resources. PU composites were prepared from castor oil (CO), polyethylene glycol (PEG3000), and hexamethylene diisocyanate (HDI). CO was used as both polyol and crosslinker. Butanediol and/or low molecular weight polyethylene glycol (PEG300) were added to the reaction medium as a chain extender. As a magnetic particle, natural magnetite or carbonyl iron was used in various amounts (0–10%). Fourier transform infrared (FTIR) spectroscopy, differential scanning calorimetry (DSC), dynamic mechanical analysis (DMA), scanning electron microscope (SEM), optical microscope, and goniometer were used to characterize all composites and pure PU. A bending test was applied to investigate the shape fixity and shape recovery ratios of the samples. A range of hydrophilic/hydrophobic PU composites (water contact angle is between 56–87°) having various melting and glass transition temperatures were successfully prepared. A PU composite having a good shape recovery ratio ($R_r = 96.1\%$) in a magnetic field was prepared using 10% magnetite. The PU composites were also thermo-sensitive.

Keywords: polymer composites, magnetic polymers, polyurethanes, renewable resources, shape memory polymer

1. Introduction

Magnetorheological (MR) materials are one of the prevalent classes of smart materials used for various engineering and biomedical applications such as the real-time control of smart systems [1], magnetic hyperthermia [2], drug delivery [3, 4], biosensors [5, 6], anti-radar camouflage [7] and vibration/noise control [8]. Generally, to prepare an MR material, micron- or nano-sized magnetic particles are either dispersed into [9, 10] or chemically crosslinked to [5, 6, 11, 12] a non-magnetic carrier material such as oil, gel, or elastomer. MR gels and elastomers are of great interest for various applications to eliminate the settling problem of magnetic particles [13]. To obtain a homogeneous dispersion of the particles in the polymer matrix, generally, in situ polymerization is a

much more preferable method than mechanically mixing [11, 14–16].

Besides vinyl polymers [5, 17–19], polyurethane (PU) is one of the most common polymers used to incorporate magnetic particles into the matrix [8, 13, 17, 20–22] due to its unique structure containing soft and hard segments [23]. By combining mechanical strength and shape memory response [24, 25], this unique structure offers a wide range of applications [26, 27]. There are also some commercial products produced from a blend of PU and acrylate oligomers to use as printer ink in 3D printers [28]. Researchers showed that they exhibit a good triple-shape memory response.

Shape memory polymers can change their shape from a temporary shape to an original shape with

*Corresponding author, e-mail: guners@itu.edu.tr

© BME-PT

temperature change or under electrical and magnetic fields [4, 22, 26–33]. Most shape-memory PUs are thermally activated by varying the ambient temperature. In some applications, such as in-body uses, direct heating, and overheating are not desired to induce the material due to their negative effect on tissues and organs. To overcome these problems, magnetic-field-sensitive shape memory PUs have been developed as an alternative to heat-induced materials [34]. Magnetic-field-sensitive PU composites have been successfully synthesized as shape-memory materials [15, 21, 22, 35] and as damping materials [8]. Cai *et al.* [15] prepared poly(ϵ -caprolactone)-PU-based shape memory nanocomposites by *in situ* polymerization. They reported that the shape memory nanocomposites exhibited a high shape recovery ratio at 45 °C and under a magnetic field. In another study, magnetically-sensitive PU nanocomposites, crosslinked with carbon nanotubes, were synthesized via *in situ* polymerization [35]. The shape recovery ratio of these materials was reported to be over 95% in the alternating magnetic field. Yang *et al.* [8] investigated the damping behaviors of PU-based MR gels. They determined the effect of the magnetic particle content on the mechanical performance of the gels. They used carbonyl iron as a magnetic particle. According to their results, the loss factor of MR gels, which provides information about the mobility of the polymer chain, decreased with increasing the magnetic particle content. Among the research mentioned above, only Yang *et al.* [8] used a bio-based monomer to synthesize magnetic-field-sensitive PU composites. They used castor oil (CO) as a polyol source.

Due to environmental and biological constraints, a lot of effort has been devoted to the development of bio-based shape memory PUs for food and medical applications. As indicated in the literature, shape memory PUs were successfully synthesized from natural oils such as CO [36, 37]. Calvo-Correas *et al.* [38] synthesized bio-based PUs using CO and L-lysine amino acid for biomedical applications. In our previous studies, a series of non-toxic PU films were prepared from CO and polyethylene glycol (PEG) with high shape memory performance for biomedical and food packaging applications [24, 39, 40]. All these studies mentioned above are about thermo-sensitive PUs.

As the main contribution to the literature, an easy *in situ* polymerization method was described in this

study to prepare PU composites showing shape memory behavior under a magnetic field. One of our main aims is to use renewable sources in PU composite formulation. For this purpose, CO, obtained from *Ricinus communis* (castor oil plant) in the spurge family, is used as both polyol and crosslinker. In addition, one of the magnetic particles used in the study was natural Fe₃O₄. PEG was also preferred in polymer synthesis due to its biocompatibility and wide use in biomedical and industrial applications, although it is derived from petroleum. A series of PU composites were synthesized in two different formulations in various amounts of magnetic particles (0–10%). Their glass transition temperatures were below room temperature, and their melting temperatures were between 31.5–43.5 °C. The surface water contact angle of the PU composites was measured between 56–87°. According to the bending test applied to investigate their shape memory performance, the PU composite containing 10% magnetite achieved a good shape recovery ratio ($R_r = 96.1\%$) in the magnetic field. Overall, we achieved promising results for our new magnetic-field-sensitive crosslinked shape-memory polyurethane composites.

2. Experimental studies

2.1. Materials

PEG having 3000 g·mol⁻¹ molecular weight (PEG3000) and CO (hydroxyl number ≥ 160 and acid number ≤ 1) were purchased from Sigma-Aldrich (Darmstadt, Germany), and it used as polyol sources. 1,4-Butanediol (BDO, 99%, Sigma-Aldrich, Darmstadt, Germany) and PEG with a molecular weight of 300 g·mol⁻¹ (PEG300, Sigma-Aldrich, Darmstadt, Germany) were used as chain extender. 1,6-Hexamethylene diisocyanate (HDI, Merck, Darmstadt, Germany) was used as an isocyanate source. Natural magnetite (Fe₃O₄) at around 28 μm in size was provided by Uysal Mining Company (Tekirdağ, Turkey), and carbonyl iron (micro powder iron S-1281, 4–6 μm with silica additive) was procured from ISP Technologies (Wayne, USA).

2.2. Synthesis of polymer composites

All composites were prepared using a one-step bulk polymerization technique without using any solvent or catalyst. All materials were dried before use. PEG3000 was dried in a rotary evaporator for 6 h at 90 °C. CO, magnetite, and carbonyl iron particles were dried at 80 °C under vacuum for 24 h. BDO

and PEG300 were also dried at 50 °C under a vacuum for 24 h.

In the first step of PU synthesis, a calculated amount of the PEG and CO were added to a reaction flask and mixed for 2 h at 90 °C to homogenize the mixture. Then, BDO and magnetite or carbonyl iron were added to the mixture. The reaction flask was equipped with a mechanical stirrer, N₂ inlet, and outlet. After the temperature dropped to 50 °C, HDI was slowly added to the flask and stirred for 30 minutes under a nitrogen atmosphere. The reaction mixture was first heated to 70 °C, held at this temperature for 20 min, then heated to 80 °C, and kept there for 5 min. Then, the mixture was transported into a petri dish and was held in an oven at 80 °C for 24. The reaction was monitored by Fourier transform infrared (FTIR) spectroscopic analysis. The disappearance of the absorption peak at about 2260 cm⁻¹, assigned to the free isocyanate group, was used to confirm that diisocyanate groups were completely consumed in the reaction. The thickness of the dry PU films was about 1±0.052 mm. The samples were designated as PU-*a*-*X*, where *a* indicates the type of the magnetic particles (*A* for carbonyl iron and *B* for magnetite) and formulation of the PU matrix, and *X* indicates the weight percentage of the magnetic particles in the composites.

The PU matrix was mainly synthesized in two different formulations shown in Table 1. The weight ratio of PEG to CO was equal in both formulations. The amount of chain extender in the polyol mixture is 45% by weight in the *A*-type composite and 45% by a mole in the *B*-type composite. Equivalent amounts of diisocyanate and hydroxyl components were used in both formulations. The hard segment

content (HSC) of PUs is calculated using Equation (1):

$$\text{Hard segment content [wt\%]} = \frac{W_{\text{BDO}} + W_{\text{HDI}} + W_{\text{PEG300}}}{W_t} \cdot 100 \quad (1)$$

where W_{BDO} , W_{HDI} , and W_{PEG300} are the weight of the BDO, HDI, and PEG300, respectively, and W_t is the total weight of monomers in PU formulation.

2.3. Characterization

FTIR analysis was carried out on a Spectrum One model FTIR spectrometer (PerkinElmer, Connecticut, USA) between 650 and 4000 cm⁻¹ using attenuated total reflection (ATR) mode.

Thermal properties were determined using a Diamond model differential scanning calorimetry (DSC, PerkinElmer, Massachusetts, USA) at temperatures between -65 and 350 °C with a 20 °C·min⁻¹ scanning rate under the nitrogen atmosphere.

Thermal gravimetric analyses (TGA) were carried out under a nitrogen atmosphere using a Diamond model TGA (PerkinElmer, Massachusetts, USA). The samples were heated from room temperature to 500 °C with a 20 °C·min⁻¹ heating rate.

The viscoelastic properties of the PU films were determined by a Diamond model dynamic mechanical analysis (DMA, PerkinElmer, Massachusetts, USA). The relaxation spectrum was scanned from -60 to 40 °C with a frequency of 1 Hz and a heating rate of 3 °C·min⁻¹.

A JEOL JSM 6390-LV model scanning electron microscope (SEM, Jeol, Tokyo, Japan) was employed to analyze the polymer surface. In addition, pictures

Table 1. Formulation of PU composite.

Code	Percentage of hydroxyl groups [mol%]*				HSC [wt%]	Iron particles used	
	PEG3000	CO	PEG300	BDO		Type	Amount [wt%]
PU-A-0	1.7 (27.5)	7.2 (27.5)	–	91.1 (45)	72.5	Carbonyl iron	0
PU-A-3							3
PU-A-10							10
PU-B-0	10.3 (46.6)	44.7 (46.6)	2.2 (1.0)	42.8 (5.8)	53.4	Magnetite	0
PU-B-1							1
PU-B-3							3
PU-B-5							5
PU-B-7							7
PU-B-10							10

*The initial amount of polyol in the reaction mixture is given in parenthesis as a weight percentage.

of the composite surface were taken with an optical microscope, OLYMPUS BX51 objective 10X (Olympus Global, Tokyo, Japan).

The swelling ratio of the samples was determined according to the American Society for Testing and Materials (ASTM) D570 standard. The samples were dried in an oven at 65 °C for 24 h and kept in a desiccator for 24 h. Then, the dry samples were soaked in distilled water for 4 days at 37 °C. Consequently, the swollen samples were weighed, and the swelling percentage was calculated in two ways using Equation (2) and Equation (3):

$$\text{Swelling ratio [wt\%]} = \frac{W_S - W_D}{W_D} \cdot 100 \quad (2)$$

$$\begin{aligned} \text{Swelling ratio (particle free) [wt\%]} &= \\ &= \frac{W_S - W_D}{W_D - W_{MP}} \cdot 100 \quad (3) \end{aligned}$$

where W_S and W_D are the weight of the swollen and dry samples, respectively, and W_{MP} is the weight of magnetic particles in the sample formulation.

Contact angle measurement was performed using a Tensiometer (CAM 200, KSV Instruments, Helsinki, Finland) at room temperature. The sessile drop method was used to measure the contact angle directly. For this purpose, the PU film was placed on the equipment platform, and then a 5 μ l droplet of distilled water was gently settled on the sample surface with the help of an automatic dispenser. The contact angle due to intermolecular cohesion and adhesion forces was determined using the software.

The density of composite films was determined by Precisa XB 220 density meter (Precisa Gravimetrics AG, Dietikon, Switzerland).

A Hot Disk TPS 2500 S model thermal conductivity analyzer (Hot Disk AB, Gothenburg, Sweden) was used to measure the absolute thermal conductivity of the composites at 25 °C.

2.4. Shape memory properties

The bending test investigated the shape memory properties of the composites under the influence of the magnetic field [14]. For this purpose, a composite sheet was cut in 50×10 mm (original shape) from the PU sample. In the programming step, the composite sheet was firstly heated to 65 °C and held there for 5 min, then bent to an angle θ_{max} by applying 2 kg mass. Next, the bent sample was cooled to +4 °C

and held for 5 min. Thus, the temporary shape of the sample was fixed. After that, the force was released, and the angle was remeasured and recorded as θ_{fixed} . In the shape recovery step, the sample recovered its original shape under the magnetic field at a frequency of 133.7 kHz and a power of 5 kW. The final angle reached after recovery was designated as θ_{final} .

The shape recovery properties of each sample were also investigated by direct heating. Again, the bending test was used to determine the performance of the sample. This was accomplished by heating the sample to 40 or 65 °C in an oven for 5 min and measuring the final angle (θ_{final}) reached after recovery. All measurements were done at least three times with three different pieces, and the average was reported.

Shape fixity (R_f) and shape recovery (R_r) ratios were calculated according to Equation (4) and Equation (5), respectively:

$$R_f [\%] = \frac{\theta_{\text{fixed}}}{\theta_{\text{max}}} \cdot 100 \quad (4)$$

$$R_r [\%] = \frac{\theta_{\text{fixed}} - \theta_{\text{final}}}{\theta_{\text{max}}} \cdot 100 \quad (5)$$

3. Results and discussion

In our previous study [24], we prepared a series of shape memory PU films synthesized from CO and PEG with different molecular weights (1500, 3000, and 8000 $\text{g}\cdot\text{mol}^{-1}$) of PEG and different weight ratios (50/50, 60/40, or 70/30) of CO to PEG. After a detailed characterization of the samples, the PU composite prepared with PEG3000 in a CO/PEG weight ratio of 50/50 was chosen as a promising candidate for biomedical applications due to its ideal transition temperature at about 39 °C and good shape memory performance. Furthermore, its shape recovery ratio was determined in the air and the phosphate buffer solution to be 96 and 88%, respectively. In addition, it was non-toxic to NIH 3T3 cells. Based on these results, in the present study, we mainly focused on preparing a new magnetic-field-sensitive crosslinked shape-memory PU composite using natural magnetite or carbonyl iron.

In order to investigate the effects of the type and the percentage of magnetic particles on the shape memory performance of the composites, two types of PU composites were prepared: *A*-type composites, which were prepared by using carbonyl iron particles, and

B-type composites, which included natural magnetite type iron particles. There was a ratio of 3 to 10% of magnetic particles in the former and a range of 1–10% in the latter. In addition, as reported in the literature [41], PEG300 was also used together with BDO to enhance the flexibility of *B*-type composites.

3.1. Polymer synthesis and characterization

FTIR spectra of *A*-type composites (PU-A-3 and PU-A-10) and pure polyurethane (PU-A-0) are shown in Figure 1. The FTIR spectrum of the reaction mixture to synthesize pure polyurethane is also seen in the figure. As a result of the consumption of HDI and polyols and synthesis of PU, the absorption peaks at 2264 cm^{-1} (assigned to the N=C=O group) and 3410 cm^{-1} (assigned to the OH group) disappeared, and 3320 cm^{-1} (assigned to the NH group) appeared. All reactions were monitored by this method.

The peaks at 2930 and 2858 cm^{-1} are CH stretching and CH_3 bending characteristic peaks, respectively. The peak at around 1683 cm^{-1} wavelength shows the amide-I region C=O stretching movement. The peaks at around 1742 and 1536 cm^{-1} are the non-hydrogen

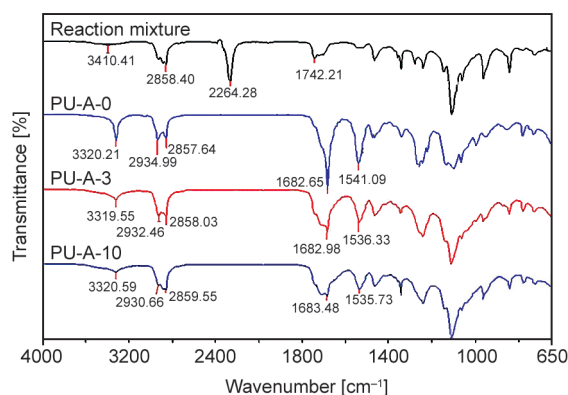


Figure 1. FTIR spectra of the PU films.

bonded C=O stretching and the C–N stretching, respectively. According to FTIR results, the PU films were successfully prepared.

3.2. Thermal and viscoelastic properties of the composites

The thermal properties of the composites are given in Table 2. As seen, glass transition temperatures (T_g) of all composites are lower than 0°C , indicating that they are rubbery at room temperature. According to DSC results, an increase in the amounts of magnetic particles in the polymer matrix caused a decrease in the glass transition temperature. These results may be attributed to the positive effect of magnetic particles in facilitating heat transfer and regional chain mobility. Thermal conductivity measurements also confirmed this result for the PU-B-X composites. As shown in Table 2, the thermal conductivity of the composites increased with increasing the amounts of magnetite particles in the polymer matrix. A similar trend was also reported by Razzaq *et al.* [34]. The thermal conductivity of a PU composite increased from 0.2 to $0.7\text{ W}\cdot\text{m}^{-1}\cdot\text{K}^{-1}$ in addition to 40% of magnetite filler. Additionally, in the same study, the thermal conductivity of the PU composite containing 10% of iron particles was found to be $0.25\text{ W}\cdot\text{m}^{-1}\cdot\text{K}^{-1}$. Compared with Razzaq *et al.*'s [34] result, we obtained relatively higher thermal conductivity ($0.76\text{ W}\cdot\text{m}^{-1}\cdot\text{K}^{-1}$) with the addition of a lower amount of iron particles (addition of 7 and 10% of magnetite). This result is probably due to the larger particle size of iron particles which is $28\text{ }\mu\text{m}$ for our particles and $9\text{ }\mu\text{m}$ for Razzaq *et al.*'s [34] particles.

The T_g of the polymers can also be obtained from DMA analysis. Unlike the DSC data, the T_g of the samples increased with increasing amounts of magnetic particles, and the highest T_g value was obtained

Table 2. Thermal properties of the composites.

Code	T_g [°C]		Thermal conductivity [W·m ⁻¹ ·K ⁻¹]	T_m [°C]	ΔH [J·g ⁻¹]	X_c [%]	Peak height for tan δ [-]
	DSC	DMA					
PU-A-0	-29.7	-24.9	–	43.5	40.6	24.7	0.32
PU-A-3	-35.0	-22.6	–	37.8	46.7	28.4	0.33
PU-A-10	-37.3	-20.4	–	38.9	38.9	23.6	0.35
PU-B-0	-34.7	-28.1	0.33	35.4	33.9	20.6	0.23
PU-B-1	-34.2	-24.4	0.43	33.2	35.0	21.3	0.27
PU-B-3	-35.1	-23.3	0.56	34.9	28.8	17.5	0.28
PU-B-5	-42.2	-20.3	0.56	34.3	25.8	15.7	0.31
PU-B-7	-43.9	-21.6	0.76	35.9	30.4	18.5	0.33
PU-B-10	-46.5	-19.6	0.76	31.5	29.4	17.9	0.34

for the PU composite prepared with 10% magnetite particles (Table 2). Generally, relatively higher T_g can be achieved by DMA for a polymer compared to DSC analysis [24]. During the DMA analysis, samples used in the DSC analysis were exposed to extra sinusoidal force. The addition of magnetic particles increased the strength of the polymer matrix. As a result, the force required to achieve the same deformation increased, so the T_g shifted to a higher temperature.

DSC determined the melting temperatures (T_m) of the composites. As seen in Table 2, the T_m and the crystallinity percentage (X_c) of the PU matrix tend to decrease by adding magnetic particles. The crystallinity was calculated from the ratio of melting enthalpy for PU (ΔH) to melting enthalpy of 100% crystalline PEG ($\Delta H_m(\text{PEG}) = 164.6 \text{ J}\cdot\text{g}^{-1}$) obtained from DSC measurements. Generally, the crystalline phase forms in polymer structure due to the orientation of segments and chains. In our case, the magnetic particles penetrated the polymer chains and caused a deterioration in the regular structure of the polymer matrix. Thus, the increase in the amounts of magnetic particles in PU composites decreased

the polymer crystallinity and the melting temperature. As explained above, including magnetic particles can also considerably improve the heat transfer in the polymer matrix. B-type composites had lower melting temperatures than A-type due to the existence of PEG300, which has a more flexible structure than BDO.

DMA measurements investigated the viscoelastic behaviors of all polymer composites prepared in this study. Storage modulus (E'), loss modulus (E''), and $\tan \delta (E''/E')$ curves of PU composites prepared with 0, 3, and 10% magnetic particles are given in Figure 2 to show the effect of particle amount on viscoelastic behavior. As seen in Figure 2a, E' increases with increasing the particle amount for carbonyl iron-added composites (PU-A-0, PU-A-3, and PU-A-10) at low temperatures, whereas for natural magnetite-added samples (PU-B-0, PU-B-3, and PU-B-10) E' values are almost the same level shown in Figure 2d. The particle amount also affects the E'' for PU-A-X coded samples (Figure 2b). It can be explained by the size of the particles, which is 4–6 μm for carbonyl iron and 28 μm for natural magnetite. Therefore, smaller particle size is a more substantial effect on modules.

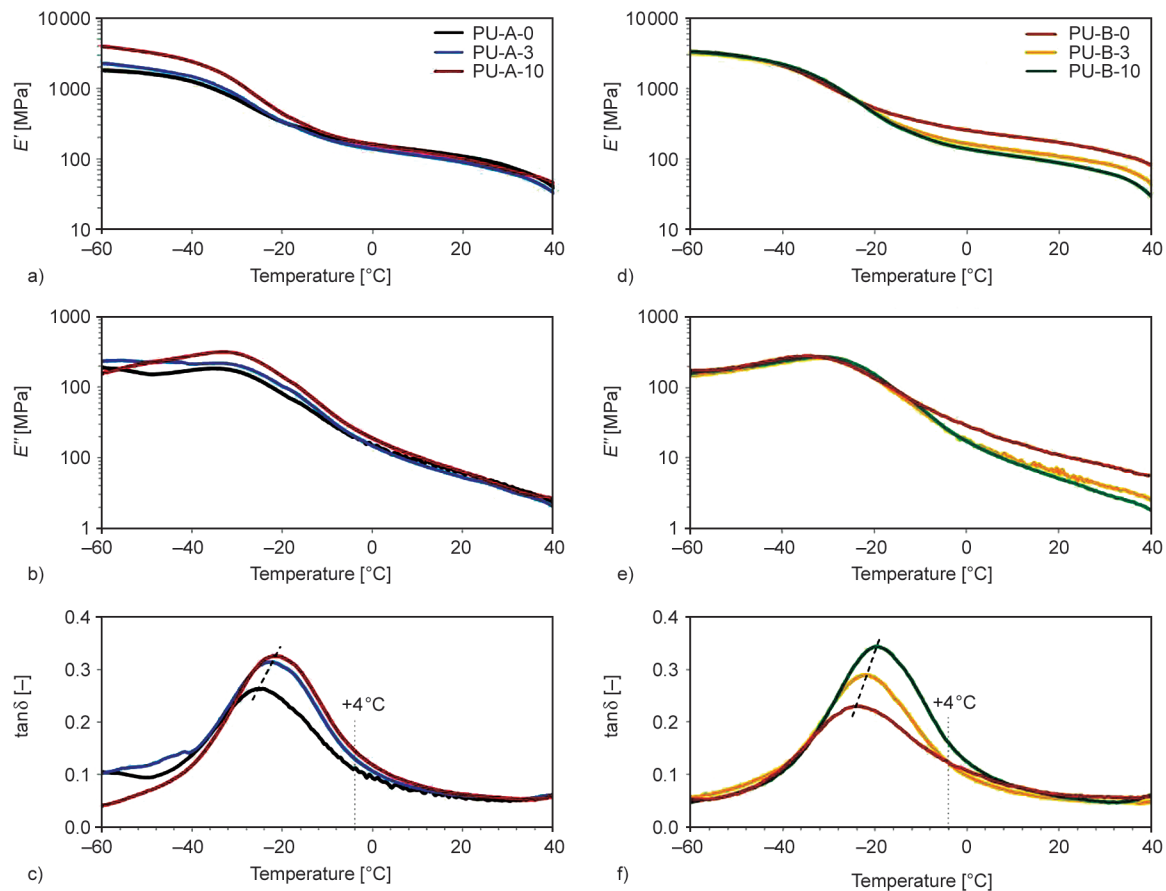


Figure 2. (a, d) Storage modulus, (b, e) loss modules and (c, f) $\tan \delta$ of the PU composites.

Additionally, almost all samples showed a sharp transition in the E'' curve, indicating high chemical resistance [34, 42].

The peak of the $\tan \delta$ curve gives the glass transition temperature (T_g) of a polymeric system. An increase in T_g in a polymer composite leads to a decrease in free volume and, therefore, a restriction of molecular motion [43]. Figures 2c and 2f show that the peak shifted to a higher temperature with increasing magnetic particles. As reported in the literature, this indicates that the loading of magnetic particles improves the elasticity of the PU composites [44], and the system had more energy dissipation potential, which provides them with good adsorption ability of shocks and vibrations [45, 46]. So, the greater the $\tan \delta$, the more dissipative the material is. Across all samples, the PU composites, including 10% of magnetic particles, displayed the highest damping capability and adding magnetic particles improves polymer composites' damping behavior.

DMA determines the T_g of neat PUs as -24.9 and -28.1 °C for PU-A-0 and PU-B-0, respectively (Table 2). PU-A-0 has a higher T_g than PU-B-0. DSC data confirmed the same trend. As explained above, increasing in T_g value is an indicator of a restriction in molecular motion. This result is probably due to the PEG content in polymer formulation. *B*-type composites have higher PEG content than *A*-type composites. It is very well known that linear-long PEG chains act as plasticizers in polymeric systems [47]. The higher PEG content causes higher chain mobility. Besides its lower PEG content, the HSC percentage of the *A*-type composite is higher than PU-B-0. The hard segments of the polyurethane limit the chain mobility [48].

TGA analyses were conducted from room temperature to up to 500 °C to determine the organic and inorganic contents of the composites. Additionally, the thermal resistance of the composites was also investigated by using this method. The results are given in Table 3. The temperature at which the addition of magnetic particles to the polymer decreased 10% weight loss. 10 and 50% weight loss for *B*-type composites occurred at lower temperatures than for *A*-types. At the final temperature of 500 °C, the weight losses were higher than 99% for pure PUs. As expected, the weight loss at 500 °C decreased with increasing the particle content for both composite types. According to the obtained data, the procedure of the composite preparation was successfully applied, and

Table 3. Results of TGA analyses of PU composites.

Code	Temperature [°C]		Weight loss at 500 °C [%]
	10% Weight loss	50% Weight loss	
PU-A-0	339.9	420.2	99.2
PU-A-3	329.1	418.1	97.4
PU-A-10	330.2	420.9	89.8
PU-B-0	329.8	408.9	99.4
PU-B-1	326.6	412.0	98.5
PU-B-3	321.9	409.4	95.5
PU-B-5	321.3	409.0	94.7
PU-B-7	318.0	410.6	93.0
PU-B-10	317.2	410.7	89.3

magnetic particles could be homogeneously dispersed in the polymer matrix.

3.3. SEM and optical microscopy images of composites

The photographs of the PU films are given in Figure 3. As shown, the PU-B-0 sample, a yellowish transparent film, turned black after adding the magnetite. Overall, homogenous composite films could be prepared on a macro-scale.

The optical microscopic images of the dry and swollen *B*-type composites obtained in the same magnification are given in Figure 4. The black areas show the presence of magnetite particles. The distribution of magnetic particles at low concentrations tended to deteriorate slightly at higher concentrations. Therefore, the images of swollen samples are more bright than dry counterparts. The best particle distribution was achieved for 1% particle content. However, the distribution was acceptable even at high concentrations.

Surface and cross-sectional SEM images of the PU samples are given in Figure 5. Surface images (Figure 5a–5f) demonstrate a rough ridge-and-valley structure of PU films. Also, it was observed that the formation of a flower pattern on the polymer surface became more regular for polymer composites due to

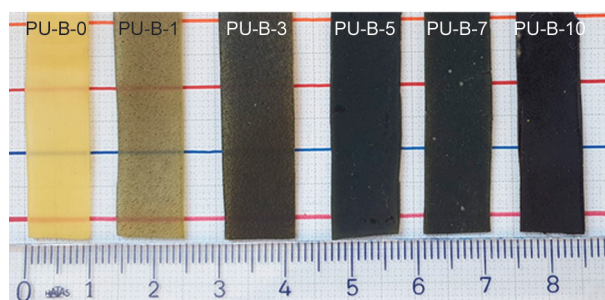


Figure 3. The photographs of the PU films.

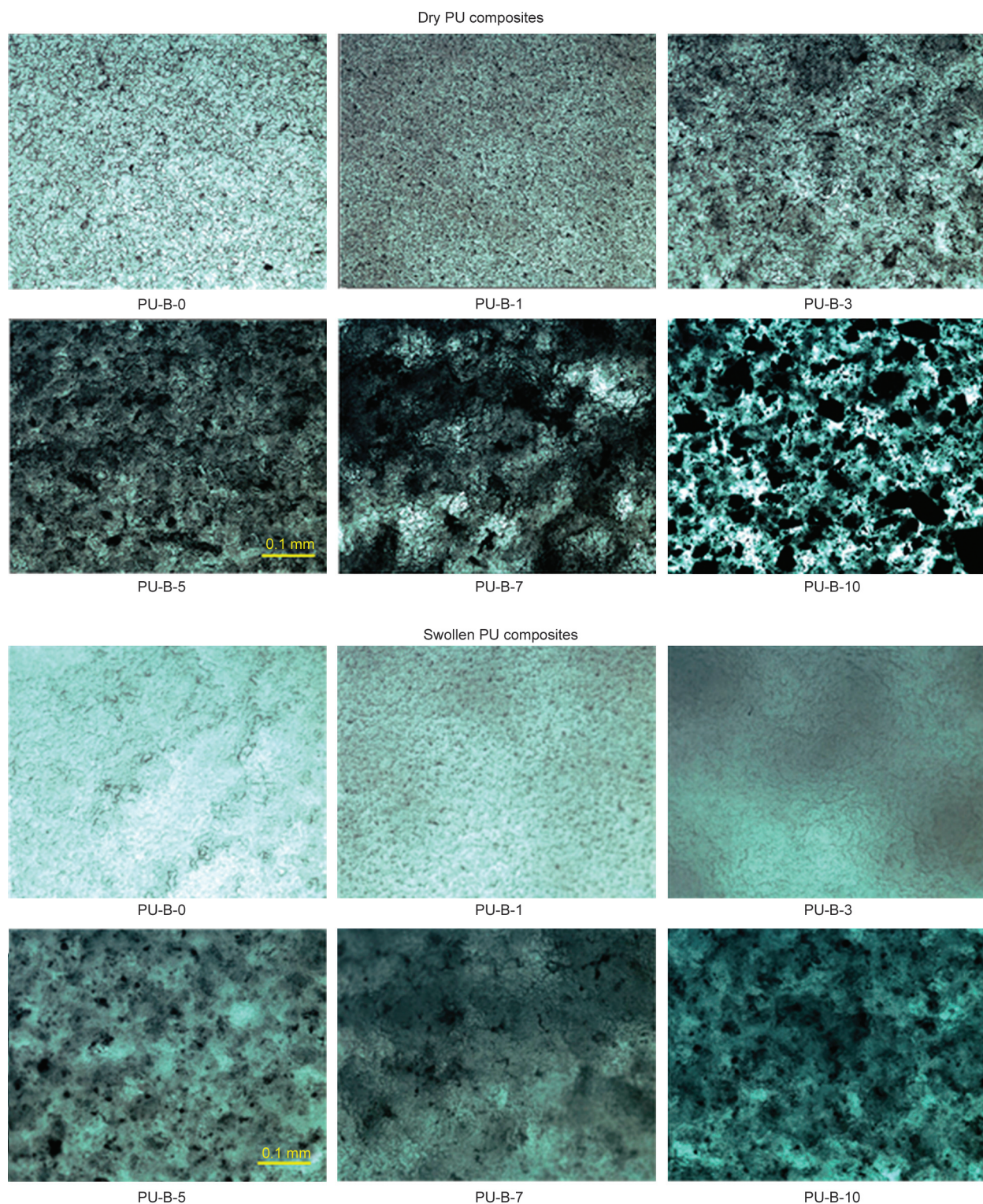


Figure 4. Optical microscopy images of dry and swollen PU composites.

the iron particles dispersed in the polymer matrix. Cross-sectional SEM images (Figures 5g and 5h) revealed that the iron particles (the red arrow refers to embedded iron particles) were distributed in the polymer matrix, in line with the results of optical microscopic observations.

3.4. Swelling properties, contact angle, and density of composites

The swelling ratios of the pure polymers and composites are given in Table 4. These values were calculated by dividing the weight of the sample by the weight of the absorbed water. The swelling ratio was

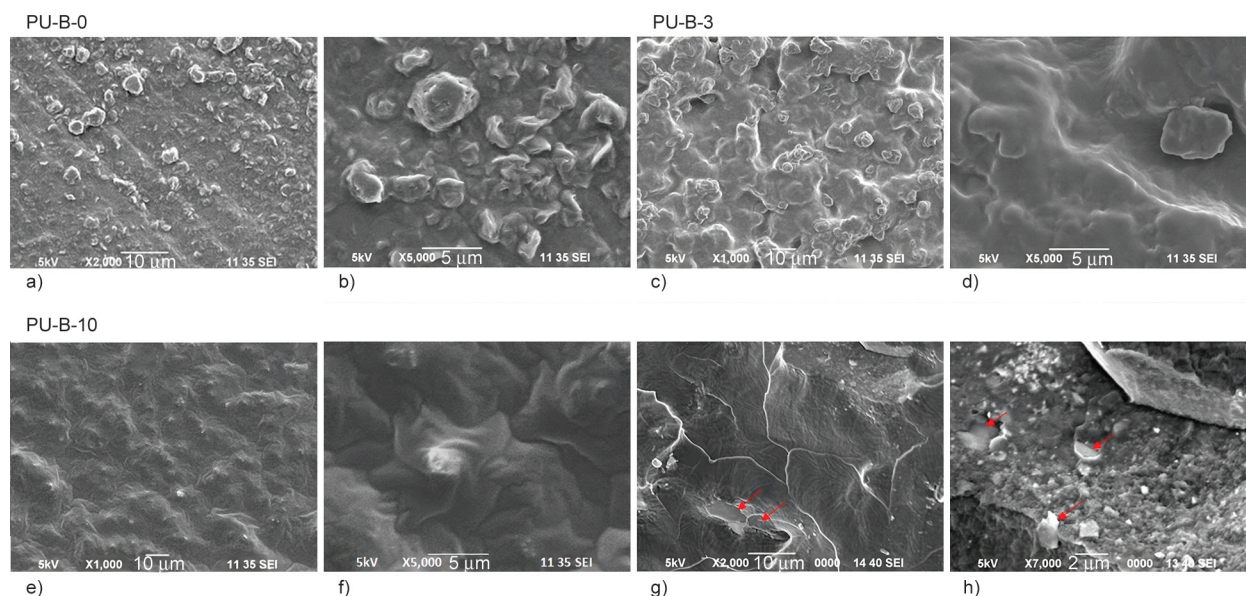


Figure 5. (a–f) Surface and (g, h) cross-sectional SEM images of PU samples.

Table 4. Swelling ratio, gel content, contact angle, and density of the composites.

Code	Swelling ratio [%]	Particle-free swelling ratio [%]	Contact angle [°]	Density [g·cm ⁻³]
PU-A-0		71.0	65.4±1.1	1.086
PU-A-3	61.9	63.7	67.9±0.8	1.095
PU-A-10	51.6	57.3	56.0±1.4	1.172
PU-B-0		73.9	64.3±1.2	1.051
PU-B-1	69.8	70.5	87.6±1.3	1.072
PU-B-3	61.8	65.3	93.9±0.9	1.106
PU-B-5	56.3	60.4	91.8±1.1	1.136
PU-B-7	57.4	61.7	93.5±0.8	1.163
PU-B-10	51.2	57.1	86.9±1.5	1.277

also calculated for each composite, excluding the weight of the magnetic particles. The pure polymers had the highest swelling ratios. As might be expected, the swelling ratio decreased with an increase in the percentage of particles for both polymer series. The swelling ratio of pure polymer B was slightly higher than that of polymer A due to the existence of PEG300 in the former one. These results suggest that the magnetic particles retain less water than the polymer. On the other hand, the swelling ratios of the composites calculated on a particle-free basis were still lower than that of pure polymers. This result may be interpreted that magnetic particles prevented polymer relaxation.

The contact angle analysis results may provide valuable information about the protein adsorption of a polymer surface when the material is used in biomedical applications. Hydrophobic surfaces have more affinity to proteins than hydrophilic surfaces [23]. In some applications, protein adsorption is a

preferable property for a biomaterial, for example, wound treatment, but in some applications, protein adsorption of the material is undesirable. As seen in Table 4, carbonyl iron particles decreased the surface contact angle. On the other hand, natural magnetite addition caused a significant increase in contact angle. These results indicate that, unlike carbonyl iron particles, magnetite particles may enhance the ability of the protein adsorption of the polymer surfaces in a biological medium.

The density of the samples is also given in Table 4. As expected, the densities of the composites are higher than that of pure PU, and they increase as the number of magnetic particles increases.

3.5. Shape memory properties

The bending test determined the composites' shape fixity (R_f) and shape recovery (R_r) ratios. Firstly, the film was heated to 65 °C and bent, applying a known force. Then, the bent film was cooled to +4 °C to fix

its temporary shape. In the final step, a magnetic field or heat was applied after removing the force, and R_f was determined. The shape-fixity temperature was chosen as +4 °C because our previous results indicated that the PEG-based hydrogels displayed a better shape memory at low temperatures [24]. The test results are given in Table 5.

The R_f was measured between 87.8–95.3% for all samples. According to the results, the R_f decreased with increasing concentration of magnetic particles for both composite types. It shows the increasing motion of polymer molecules with increasing particle amounts. This may be because the magnetic particles positioning between the chains inhibit the hydrogen bonds between the hard segments. DMA data also supports this comment that $\tan \delta$ shown in Figures 2c and 2f is the highest for the composites having the highest magnetic particle content in each series of PU at +4 °C, which is the temperature applied for shape fixity. It indicates decreasing flexibility and increasing viscous behavior of the composite with increasing magnetic particle amount.

The shape recovery of all composites was determined either under a magnetic field or directly heated at two different temperatures of 40 and 65. 40 °C is the average of the melting temperatures of composites measured in the range of 31.5 and 43.5 °C. The results obtained at this temperature allow us to evaluate the potential use of the samples in biomedical applications. The shape recovery tests were also conducted at 65 °C to compare the results of this study with our previous findings [24].

As seen in Table 5, the R_r of the composites was measured between 78.2–98.1%. B-type composites had better shape recovery performance than A-type samples

under all test conditions due to their formulation. It is well known that the hard domains of a segmented PU consist of a rigid diisocyanate, a low molecular weight (generally below 500 g·mol⁻¹) diols, or amines as a chain extender and/or crosslinker [49]. Hard domains are responsible for memorizing the material's permanent shape [50, 51]. The hard segment content (HSC) and crosslink density are major factors behind the shape memory performance of a PU material. HDI, BDO, CO, and PEG300 form the hard segments. CO was used as a crosslinker in our study. As shown in Table 1, the HSC is calculated as 72.5% for A-type composites and 53.4% for B-type composites. According to this result, the expectation is that A-type materials should perform better shape memory performance.

On the other hand, the amount of crosslinker is much higher in B-type composites (44.7% by weight) than in A-type composites (7.2% by weight). This result explains why B-type materials show a better shape recovery ratio. The positive influence of crosslink density on the shape recovery behavior of a material is also reported by Calvo-Correas *et al.* [38].

The samples in higher magnetite amounts have good shape recovery ratios ($R_r = 86.9\%$ for PU-B-7 and 96.1% for PU-B-10) in the magnetic field.

Our results are consistent with the literature. Cai *et al.* [15] reported the shape recovery ratios varying in the range of 94–98% for poly(ϵ -caprolactone)-polyurethane nanocomposites in the alternating magnetic field. The nanocomposites were proposed as potential magnetic-sensitive shape-memory materials for biomedical applications. Wang *et al.* [17] reported 97.5% of the shape recovery ratio for the poly(styrene-*b*-butadiene-*b*-styrene) copolymer/linear low-density polyethylene/Fe₂O₃ composites with the addition of 9% magnetic particles. In the case of 18% of particle addition, 99% of shape recovery was obtained. On the other hand, Calvo-Correas *et al.* [38] obtained thermally induced PUs from CO and L-lysine amino acid (LDI) as a shape-memory material. They synthesized crosslinked polymers in various monomer ratios for biomedical applications. They reported that R_f and R_r values are between 72.0–96.9 and 72.4–100%, respectively. Compared to the literature, we obtained similar results under the magnetic field.

We also investigated the contribution of magnetic particles to the shape memory performance of the

Table 5. Shape memory performance of the composites.

Code	R_f [%]	R_r [%]		
		at 40 °C	at 65 °C	Under the magnetic field
PU-A-0	94.0	87.0	91.7	–
PU-A-3	93.8	87.0	92.7	83.9
PU-A-10	90.9	92.3	96.8	86.4
PU-B-0	95.3	88.4	94.4	–
PU-B-1	94.4	83.5	94.7	78.2
PU-B-3	93.6	84.6	92.3	86.4
PU-B-5	93.3	92.0	91.7	91.5
PU-B-7	91.6	87.4	95.8	86.9
PU-B-10	87.8	93.5	98.1	96.1

PU composites when thermally induced. As shown in Table 5, R_r for both types of composites at 40 and 65 °C tends to increase with increasing amounts of magnetic particles. When the results are evaluated together with our previous findings [24], in this study, we obtained relatively higher R_r values than those of the previous one at 65 °C, most probably due to the increased thermal conductivity of the samples. In brief, we showed that adding magnetic particles positively affects the shape recovery of the materials even when thermally induced.

The shape recovery performances of the B-type composites were tested in 10 consecutive cycles. For this purpose, the sample was first programmed, then heated to 65 °C in the shape recovery step, and reprogrammed. Results are presented in Figures 6 and 7. As seen in Figure 6, the shape fixity of some composites remained fairly stable and not affected by the number of cycles, while others have fixity considerably fluctuating as a function of cycle number. However, all composites endured the test cycles with drop-in fixity of less than 10%.

As seen in Figure 7, the shape recovery tends to decrease with cycle number continuously but at a considerably low pace for most composites. For example, after 10 cycles, the decrease in the shape recovery ratios of the pure polymer and three composites was

less than about 5%, while PU-B-3 and PU-B 5 suffered a drop of about 20%.

4. Conclusions

In this study, a series of PU composites were synthesized from castor oil, PEG3000, hexamethylene diisocyanate, butanediol, and/or PEG300 via in situ polymerization. Natural magnetite or carbonyl iron was added to the reaction medium in various amounts as magnetic particles. After the characterization of all samples using various methods, their shape memory performances were determined by bending tests in magnetic fields. Shape fixity decreased with increasing amounts of magnetic particles. On the other hand, shape recovery increased with increasing concentration of magnetic particles. Magnetite-added samples showed a higher shape recovery ratio. After evaluating all results, we supposed that 10% of magnetic particle added PU composite has the highest damping capability. This formulation can be used as a new magnetic material in various engineering applications.

Acknowledgements

Preliminary experiments of this work were supported by the State Planning Organization of Turkey [Project Number 90186] and the Istanbul Technical University Scientific Research Project Foundation (ITU BAP) [Project Number 36166]. The authors thank Assoc. Prof. Fatma Elif Genceli Güner for the optical microscopy images.

References

- [1] Sohn J. W., Kim G-W., Choi S-B.: A state-of-the-art review on robots and medical devices using smart fluids and shape memory alloys. *Applied Sciences*, **8**, 1928 (2018).
<https://doi.org/10.3390/app8101928>
- [2] Kumar C. S. S. R., Mohammad F.: Magnetic nanomaterials for hyperthermia-based therapy and controlled drug delivery. *Advanced Drug Delivery Reviews*, **63**, 789–808 (2011).
<https://doi.org/10.1016/j.addr.2011.03.008>
- [3] Zhao F., Yao D., Guo R., Deng L., Dong A., Zhang J.: Composites of polymer hydrogels and nanoparticulate systems for biomedical and pharmaceutical applications. *Nanomaterials*, **5**, 2054–2130 (2015).
<https://doi.org/10.3390/nano5042054>
- [4] Meng H., Li G.: A review of stimuli-responsive shape memory polymer composites. *Polymer*, **54**, 2199–2221 (2013).
<https://doi.org/10.1016/j.polymer.2013.02.023>

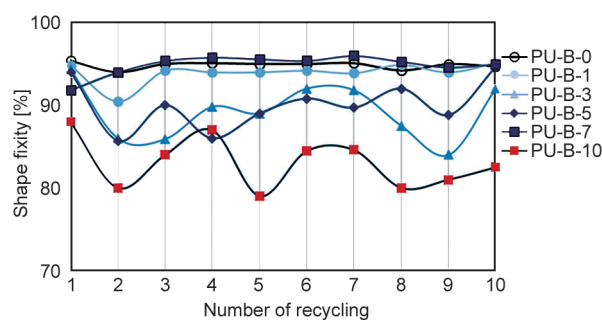


Figure 6. Changes in the shape fixity ratio in multiple bending test cycles.

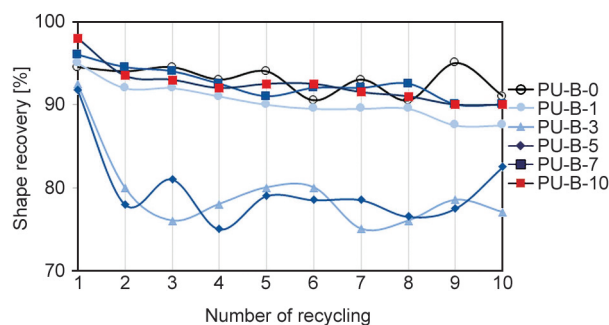


Figure 7. Changes in the shape recovery ratio in multiple bending test cycles.

- [5] Blyakhman F. A., Buznikov N. A., Sklyar T. F., Safronov A. P., Golubeva E. V., Svalov A. V., Sokolov S. Y., Melnikov G. Y., Orue I., Kurlyandskaya G. V.: Mechanical, electrical and magnetic properties of ferrogels with embedded iron oxide nanoparticles obtained by laser target evaporation: Focus on multifunctional biosensor applications. *Sensors*, **18**, 872 (2018).
<https://doi.org/10.3390/s18030872>
- [6] Kurlyandskaya G. V., Fernández E., Safronov A. P., Blyakhman F. A., Svalov A. V., Burgoa Beitia A., Beketov I. V.: Magnetoimpedance biosensor prototype for ferrogel detection. *Journal of Magnetism and Magnetic Materials*, **441**, 650–655 (2017).
<https://doi.org/10.1016/j.jmmm.2017.06.073>
- [7] Yu M., Zhu M., Fu J., Yang P. A., Fu J., Qi S.: A dimorphic magnetorheological elastomer incorporated with Fe nano-flakes modified carbonyl iron particles: Preparation and characterization. *Smart Materials and Structures*, **24**, 115021 (2015).
<https://doi.org/10.1088/0964-1726/24/11/115021>
- [8] Yang P., Yu M., Fu J., Liu S., Qi S., Zhu M.: The damping behavior of magnetorheological gel based on polyurethane matrix. *Polymer Composites*, **38**, 1248–1258 (2017).
<https://doi.org/10.1002/pc.23689>
- [9] Golbang A., Kokabi M.: Temporary shape development in shape memory nanocomposites using magnetic force. *European Polymer Journal*, **47**, 1709–1719 (2011).
<https://doi.org/10.1016/j.eurpolymj.2011.06.008>
- [10] Chen J., Zhang G-X., Jin J.: Preparation and deflection characterization of intelligent polymer gels controlled by magnetic fields. in ‘2007 IEEE International Conference on Robotics and Biomimetics (ROBIO). Sanya, China’, 1827–1832 (2007).
<https://doi.org/10.1109/ROBIO.2007.4522444>
- [11] Gao Y., Zhu G., Xu S., Ma T., Nie J.: Biodegradable magnetic-sensitive shape memory poly(ϵ -caprolactone)/Fe₃O₄ nanocomposites. *Journal of Applied Polymer Science*, **135**, 45652 (2018).
<https://doi.org/10.1002/app.45652>
- [12] Marcelo G., Muñoz-Bonilla A., Rodríguez-Hernández J., Fernández-García M.: Hybrid materials achieved by polypeptide grafted magnetite nanoparticles through a dopamine biomimetic surface anchored initiator. *Polymer Chemistry*, **4**, 558–567 (2013).
<https://doi.org/10.1039/C2PY20514A>
- [13] Khairi M. H. A., Mazlan S. A., Ubaidillah, Choi S-B., Abdul Aziz S. A. A., Mohamad N., Hapipi N. M., Nordin N.: Role of additives in enhancing the rheological properties of magnetorheological solids: A review. *Advance Engineering Materials*, **21**, 1800696 (2019).
<https://doi.org/10.1002/adem.201800696>
- [14] Narendra Kumar U., Kratz K., Behl M., Lendlein A.: Shape-memory properties of magnetically active triple-shape nanocomposites based on a grafted polymer network with two crystallizable switching segments. *Express Polymer Letters*, **6**, 26–40 (2012).
<https://doi.org/10.3144/expresspolymlett.2012.4>
- [15] Cai Y., Jiang J-S., Zheng B., Xie M-R.: Synthesis and properties of magnetic sensitive shape memory Fe₃O₄/poly(ϵ -caprolactone)-polyurethane nanocomposites. *Journal of Applied Polymer Science*, **127**, 49–56 (2013).
<https://doi.org/10.1002/app.36849>
- [16] Hu X., Wang Y., Xu M., Zhang L., Zhang J., Dong W.: Mechanical testing and reinforcing mechanisms of a magnetic field-sensitive hydrogel prepared by microwave-assisted polymerization. *Polymer Testing*, **71**, 344–351 (2018).
<https://doi.org/10.1016/j.polymertesting.2018.09.027>
- [17] Wang Y., Ye J., Tian W.: Shape memory polymer composites of poly(styrene-*b*-butadiene-*b*-styrene) copolymer/liner low density polyethylene/Fe₃O₄ nanoparticles for remote activation. *Applied Science*, **6**, 333 (2016).
<https://doi.org/10.3390/app6110333>
- [18] Sarıtaş S., Eşsiz S., Sarı B.: Synthesis and characterization of foldable and magnetic field-sensitive, free-standing poly(vinyl acetate)/poly(vinyl chloride)/polyfuran composite and nanocomposite films. *Journal of Magnetism and Magnetic Materials*, **433**, 120–130 (2017).
<https://doi.org/10.1016/j.jmmm.2017.03.007>
- [19] Meharthaj H., Sivakumar M. S., Arockiarajan A.: Significance of particle size on the improved performance of magnetorheological gels. *Journal of Magnetism and Magnetic Materials*, **490**, 165483 (2019).
<https://doi.org/10.1016/j.jmmm.2019.165483>
- [20] Pilate F., Toncheva A., Dubois P., Raquez J-M.: Shape-memory polymers for multiple applications in the materials world. *European Polymer Journal*, **80**, 268–294 (2016).
<https://doi.org/10.1016/j.eurpolymj.2016.05.004>
- [21] Mohr R., Kratz K., Weigel T., Lucka-Gabor M., Moneke M., Lendlein A.: Initiation of shape-memory effect by inductive heating of magnetic nanoparticles in thermoplastic polymers. *The Proceedings of the National Academy of Sciences*, **103**, 3540–3545 (2006).
<https://doi.org/10.1073/pnas.0600079103>
- [22] Huang W. M., Ding Z., Wang C. C., Wei J., Zhao Y., Purnawali H.: Shape memory materials. *Materials Today*, **13**, 54–61 (2010).
[https://doi.org/10.1016/S1369-7021\(10\)70128-0](https://doi.org/10.1016/S1369-7021(10)70128-0)
- [23] Kürkçüoğlu O., Güner F. S.: Polyurethanes: Surface protein adsorption. in ‘Encyclopedia of biomedical polymers and polymeric biomaterials’ (ed.: Mishra M.) CRC Press, Boca Raton, Vol. 9, 6724–6742 (2015).
- [24] Bonfil M., Sirkecioglu A., Bingol-Ozakpinar O., Uras F., Güner F. S.: Castor oil and PEG-based shape memory polyurethane films for biomedical applications. *Journal of Applied Polymer Science*, **131**, 40590 (2014).
<https://doi.org/10.1002/APP.40590>
- [25] Yilgör E., Yurtsever E., Yilgör I.: Hydrogen bonding and polyurethane morphology. II. Spectroscopic, thermal and crystallization behavior of polyether blends with 1,3-dimethylurea and a model urethane compound. *Polymer*, **43**, 6561–6568 (2002).
[https://doi.org/10.1016/S0032-3861\(02\)00566-9](https://doi.org/10.1016/S0032-3861(02)00566-9)

- [26] Zhang M. Q.: Shape memory polymer capable of gradual transformation and working. *Express Polymer Letters*, **16**, 1011 (2022).
<https://doi.org/10.3144/expresspolymlett.2022.73>
- [27] Wang Z., Li W., Yang X., Cao J., Tu Y., Wu R., Wang W.: Highly stretchable and compressible shape memory hydrogels based on polyurethane network and supra-molecular interaction. *MaterialsToday Communications*, **17**, 246–251 (2018).
<https://doi.org/10.1016/j.mtcomm.2018.09.006>
- [28] Dai L., Song J., Qu S., Xiao R.: Triple-shape memory effect in 3D-printed polymers. *Express Polymer Letters*, **14**, 1116–1126 (2020).
<https://doi.org/10.3144/expresspolymlett.2020.91>
- [29] Chow W. S., Mohd Ishak Z. A.: Smart polymer nanocomposites: A review. *Express Polymer Letters*, **14**, 416–435 (2020).
<https://doi.org/10.3144/expresspolymlett.2020.35>
- [30] Chen S., Hu J., Zhuo H.: Properties and mechanism of two-way shape memory polyurethane composites. *Composites Science and Technology*, **70**, 1437–1443 (2010).
<https://doi.org/10.1016/j.compscitech.2010.01.017>
- [31] Liu G., Guan C., Xia H., Guo F., Ding X., Peng Y.: Novel shape-memory polymer based on hydrogen bonding. *Macromolecular Rapid Communications*, **27**, 1100–1104 (2006).
<https://doi.org/10.1002/marc.200600189>
- [32] Behl M., Lendlein A.: Shape-memory polymers. *MaterialsToday*, **10**, 20–28 (2007).
[https://doi.org/10.1016/S1369-7021\(07\)70047-0](https://doi.org/10.1016/S1369-7021(07)70047-0)
- [33] Hu J., Zhu Y., Huang H., Lu J.: Recent advances in shape-memory polymers: Structure, mechanism, functionality, modeling and applications. *Progress in Polymer Science*, **37**, 1720–1763 (2012).
<https://doi.org/10.1016/j.progpolymsci.2012.06.001>
- [34] Razzaq M. Y., Anhalt M., Frommann L., Weidenfeller B.: Thermal, electrical and magnetic studies of magnetite filled polyurethane shape memory polymers. *Materials Science and Engineering: A*, **444**, 227–235 (2007).
<https://doi.org/10.1016/j.msea.2006.08.083>
- [35] Cai Y., Jiang J.-S., Liu Z.-W., Zeng Y., Zhang W.-G.: Magnetically-sensitive shape memory polyurethane composites crosslinked with multi-walled carbon nanotubes. *Composites Part A: Applied Science and Manufacturing*, **53**, 16–23 (2013).
<https://doi.org/10.1016/j.compositesa.2013.05.016>
- [36] Abbasi A., Sadeghi G. M. M., Ghasemi I.: Synthesis and characterization of novel environmentally friendly shape memory polyurethanes based on poly(epsilon-caprolactone) diol/castor oil mixtures. *Polymer Science Series B*, **59**, 526–536 (2017).
<https://doi.org/10.1134/S1560090417050013>
- [37] Saralegi A., Foster E. J., Weder C., Eceiza A., Corcuera M. A.: Thermoplastic shape-memory polyurethanes based on natural oils. *Smart Materials and Structures*, **23**, 025033 (2014).
<https://doi.org/10.1088/0964-1726/23/2/025033>
- [38] Calvo-Correas T., Gabilondo N., Alonso-Varona A., Palomares T., Corcuera M. A., Eceiza A.: Shape-memory properties of crosslinked biobased polyurethanes. *European Polymer Journal*, **78**, 253–263 (2016).
<https://doi.org/10.1016/j.eurpolymj.2016.03.030>
- [39] Çakmak E. G., Dalgakiran D., Güner F. S.: Castor oil and PEG-based shape memory polyurethane films: Effect of chain extender amount on some polymer properties and performance. *Turkish Journal of Chemistry*, **42**, 1161–1173 (2018).
<https://doi.org/10.3906/kim-1703-61>
- [40] Turan D., Gunes G., Güner F. S.: Synthesis, characterization and O₂ permeability of shape memory polyurethane films for fresh produce packaging. *Packaging Technology and Science*, **29**, 415–427 (2016).
<https://doi.org/10.1002/pts.2222>
- [41] Oprea S.: The effect of chain extenders structure on properties of new polyurethane elastomers. *Polymer Bulletin*, **65**, 753–766 (2010).
<https://doi.org/10.1007/s00289-009-0242-9>
- [42] Yeganeh H., Hojati-Talemi P.: Preparation and properties of novel biodegradable polyurethane networks based on castor oil and poly(ethylene glycol). *Polymer Degradation and Stability*, **92**, 480–489 (2007).
<https://doi.org/10.1016/j.polymdegradstab.2006.10.011>
- [43] Ganguli S., Roy A. K., Anderson D. P.: Improved thermal conductivity for chemically functionalized exfoliated graphite/epoxy composites. *Carbon*, **46**, 806–817 (2008).
<https://doi.org/10.1016/j.carbon.2008.02.008>
- [44] Madarvoni S., Rama S. P. S.: Dynamic mechanical behaviour of graphene, hexagonal boron nitride reinforced carbon-kevlar, hybrid fabric-based epoxy nanocomposites. *Polymers and Polymer Composites*, **30**, 1–14 (2022).
<https://doi.org/10.1177/09673911221107289>
- [45] Menard K. P.: *Dynamic mechanical analysis: A practical introduction*. CRC Press, Washington (2008).
- [46] Wei W., Zhang Y., Liu M., Zhang Y., Yin Y., Gutowski W. S., Deng P., Zheng C.: Improving the damping properties of nanocomposites by monodispersed hybrid POSS nanoparticles: Preparation and mechanisms. *Polymers*, **11**, 647 (2019).
<https://doi.org/10.3390/polym11040647>
- [47] Li F.-J., Zhang S.-D., Liang J.-Z., Wang J.-Z.: Effect of polyethylene glycol on the crystallization and impact properties of polylactide-based blends. *Polymers for Advanced Technologies*, **26**, 465–475 (2015).
<https://doi.org/10.1002/pat.3475>
- [48] Potolinca V. O., Oprea S.: New polyurethanes containing cycloaliphatic units in the hard segments. The influence of the microstructure on the thermo-mechanical and surface properties. *Polymers for Advanced Technologies*, in press (2022).
<https://doi.org/10.1002/pat.5962>

- [49] Arévalo-Alquichire S., Morales-Gonzalez M., Navas-Gómez K., Diaz L. E., Gómez-Tejedor J. A., Serrano M-A., Valero M. F.: Influence of polyol/crosslinker blend composition on phase separation and thermo-mechanical properties of polyurethane thin films. *Polymers*, **12**, 666 (2020).
<https://doi.org/10.3390/polym12030666>
- [50] Sáenz-Pérez M., Laza J. M., Garcia-Barrasa J., Vilas J. L., León L. M.: Influence of the soft segment nature on the thermomechanical behavior of shape memory polyurethanes. *Polymer Engineering and Science*, **58**, 238–244 (2018).
<https://doi.org/10.1002/pen.24567>
- [51] Saad N. M., Saridi M. H. M., Zubir S. A.: Segmented shape memory polyurethane: Influence of soft segment types and length. *MaterialsToday*, **66**, 2801–2805 (2022).
<https://doi.org/10.1016/j.matpr.2022.06.519>